Fault-Tolerant Path-Tracking Control with PID Controller for 4ws4wd Electric Vehicles

Youcef Zennir, Sami Allou, and J. J. Fernandez-Lozano

Abstract This work deals with the problem of fault path tracking for an electric vehicle which has four electromechanical wheel Systems. A controller based on tow PID the first controller for the speed and the second for the steering control to ensure that the robot follows the trajectory, during the design of this controller the effort was concentrated on the simplicity and efficiency. The processing and response time are very essential factors in the process control, which is what motivated the choices of the structure and the parameters of the different parts. The effectiveness of the proposed velocity control method is confirmed by numerical simulations.

Keywords Mobile RAMBLER robot · Modelling · PID controller · Electric vehicle · Fault-tolerant control

1 Introduction

The saturation of the road network in the city centres has become a problem, to resolve this problem and facilitate mobility it is necessary to create new networks or to use the available resources in an optimal way, but the construction of new infrastructure is not realizable all the time, so it is necessary to imagine new transport system is what motivated the researchers study all aspects of autonomous vehicles this type of vehicle has a high efficiency per a port to vehicles driven by humans The electric vehicle (EV) is a relatively new concept in the world of the automotive industry [1]. Although some companies have based their entire model of cars around being proactive and using electricity, some also offer hybrid vehicles that work off both electricity and gas. EV's get their power from rechargeable batteries installed inside the vehicle [2–4]. The electric vehicles are a great way to not only save money but

Y. Zennir (✉) · S. Allou
Automatic Laboratory of Skikda, université 20 août, 1955 Skikda, Skikda, Algeria
e-mail: y.zennir@univ-skikda.dz

J. J. Fernandez-Lozano
Departamento de Ingeniería de Sistemas y Automática, Escuela de Ingenierías Industriales, Universidad de Málaga, Calle Dr. Ortiz Ramos, Málaga, Spain

S. Bououden et al. (eds.), *Proceedings of the 4th International Conference on Electrical Engineering and Control Applications*, Lecture Notes in Electrical Engineering 682,
https://doi.org/10.1007/978-981-15-6403-1_64

also help contribute towards a healthy and stable environment. Many research works have been conducted to study electric vehicles control [5, 6], deal steering stability of platoon equipped with cooperative adaptive cruise control (CACC). In this work we started by the control of a single vehicle, we used tow PID controllers to control the vehicle one for the steering and the other one for the vehicle speed [7].

2 Modeling of Rambler

The modelling is an important step before the application of the control, the more the modelling takes into account all the forces applied on the system the more the results are efficient. The robot that we used is an autonomous electric vehicle (RAMBLER). It has been developed by the University of Malaga [1], It is a 4-motor-wheel skid-steer mobile robot, with active suspension. RAMBLER robot uses 4 in-wheel brushless motors. Each motor is controlled by an embedded board that integrates a microcontroller (μC) and an independent H-bridge power stages [8–10] (Fig. 1).

A vehicle (RAMBLER) dynamic model has been developed useful for control design, neglecting some side effects introduced, by suspensions and tire deformation.

Define a fixed reference frame f(x, u) and a moving frame f(z, y) attached to the vehicle body, with origin at the vehicle center of mass G (see Fig. 2). Let $\dot{x}$, $\dot{y}$, $\dot{\theta}$ be, respectively, the longitudinal, lateral, and angular velocity of the vehicle in frame f.

Fig. 1 Electric robot RAMBLER [1]

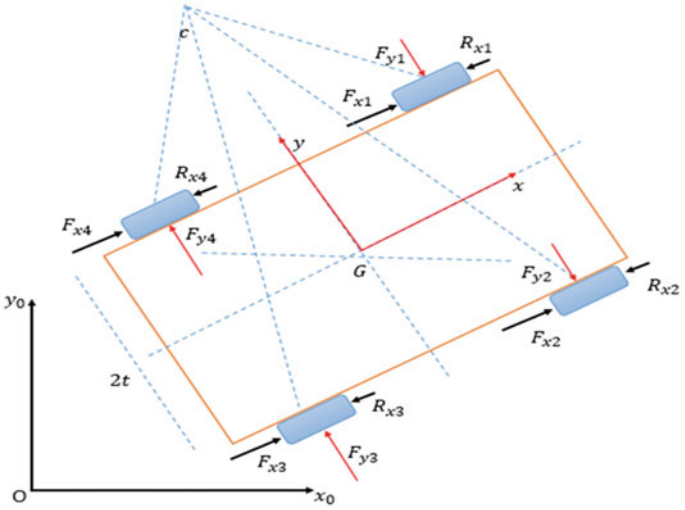

Fig. 2 Free-body diagram [7]

The free-body diagram of forces and velocities is shown in Fig. 2, with the vehicle having instantaneous positive velocity components $\dot{x}$ and $\dot{\theta}$ and negative velocity $\dot{y}$. Wheels develop tractive forces F_{xi} and are subject to longitudinal resistance forces R_{xi} for i = 1, …, 4. We assume that wheel actuation is equal on each side so as to reduce longitudinal slip. Thus, it will always be $F_{x4} = F_{x1}$ and $F_{x3} = F_{x2}$. Lateral forces F_{yi} act on the wheels as a consequence of lateral skidding. Also, a resistive moment M_r, around the center of mass is induced in general by the F_{yi} and R_{xi} forces. For a vehicle of mass m and inertia I about its center of mass, the equations of motion can be written in frame f as:

$$ma_x, = 2F_{x1} + 2F_{x2} - R_x \tag{1}$$

$$ma_v, = -F_v \tag{2}$$

$$I\ddot{\theta}, = 2t(F_{x1} + F_{x2}) - M_r \tag{3}$$

To express the longitudinal resistive force R_x, the lateral resistive force F_y, and the resistive moment M_r, we should consider how the vehicle gravitational load mg is shared among the wheels and introduce a Coulomb friction model for the wheel-ground contact. We have:

$$F_{x4} = F_{x1} = \frac{b}{a+b} \cdot \frac{mg}{2} \tag{4}$$

$$F_{x3} = F_{x2} = \frac{a}{a+b} \cdot \frac{mg}{2} \tag{5}$$

where: a: Front wheelbase; b: Rear wheel base.

At low speed, the lateral load transfer due to centrifugal forces on curved paths can be neglected. In case of hard ground, we can assume that the contact patch between wheel and ground is rectangular and that the tire vertical load produces a uniform pressure distribution. In this condition, $R_{xi} = f_r F_{zi} \mathrm{sgn}(\dot{x}_i)$ where f_r is the coefficient of rolling resistance, assumed independent from velocity. The total longitudinal resistive force is then:

$$R_x = \sum_{i=1}^{4} R_{xi} = f_r \frac{mg}{2} (\mathrm{sgn}(\dot{x}_1) + \mathrm{sgn}(\dot{x}_2)) \tag{6}$$

Introducing a lateral friction coefficient u, the lateral force acting on each wheel will be:

$$F_{yi} = u F_{zi} \mathrm{sgn}(\dot{y}_2) \tag{7}$$

The total lateral force is thus

$$F_y = \sum_{i=1}^{4} F_{yi} = u \frac{mg}{a+b} (\mathrm{sgn}(\dot{y}_1) + \mathrm{sgn}(\dot{y}_3)) \tag{8}$$

While the resistive moment is

$$\begin{aligned} M_r &= a\big(F_{y1} + F_{y2}\big) - b\big(F_{y3} + F_{y4}\big) + t[(R_{x2} - R_{x3}) - (R_{x1} - R_{x4})] \\ &= \frac{abmg}{a+b} (\mathrm{sgn}(\dot{y}_1) + \mathrm{sgn}(\dot{y}_3)) + f_r \frac{mg}{2} (\mathrm{sgn}(\dot{x}_1) + \mathrm{sgn}(\dot{x}_2)) \end{aligned} \tag{9}$$

3 Control Design

Increasingly stringent standards on vehicle emissions and fuel economy have made hybrid electric vehicles (HEVs) and/or plug-in HEVs (PHEVs) increasingly more attractive to both the industrial and academic communities Not only various HEVs and/or PHEVs, such as the Toyota Prius and the Ford Escape, have already entered mass production, but the tendency toward pure electric ground vehicles (EGVs) has also been significantly accelerated by various electrified systems and technologies instead of the conventional mechanical/hydraulic counterparts [11, 12]. For example, regenerative braking can transfer the vehicle kinetic energy into battery electrical energy during the deceleration processes and consequently reduce energy loss from

frictional heat in traditional mechanical/hydraulic brakes. In-wheel electrical motor control is also a novel technology that provides faster and more accurate torque actuation. Electric differential (ED) is another electrified technology that eliminates the traditional mechanical differentials (MDs). An ED system can reduce the weight and friction loss in the drive train by removing MD components and consequently improve the overall reliability and efficiency during the power transmission. The working principle of an ED system is similar to that of a traditional MD. When an EGV is cornering or making a turn, the outer wheels will travel longer paths than the inner ones, implying that the rotational speed of the outer wheels will be faster than that of the inner wheels. The resulting speed differences between the inner and outer wheels are automatically tuned by an ED system [12–15]. Note that an ED system in an EGV with independently actuated in-wheel motors is essentially a wheel speed tracking control module, which is different from the direct torque control of in-wheel motors.

To keep the mobile robot on our desired trajectory and desired velocity it is necessary to design a regulator which will allow tracking of arbitrary trajectories (xr (t), yr (t)). The design of controllers which we used is based on PID the first one for the speed control receives the speed error of the vehicle and the second the speed tracking, the robot speed measured by a GPS system as shown in Fig. 3, at the output of the controller, we receive the linear speed and the steering speed necessary for the robot to remain on the trajectory [16–18].

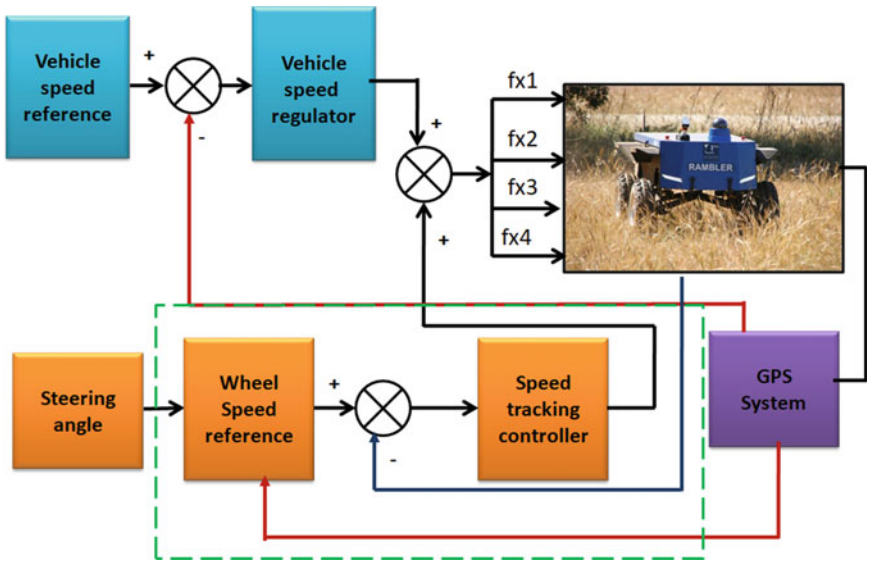

Fig. 3 Block diagram of robot control diagram

4 Simulink Model

To illustrate the proposed control for RAMBLER, we built a SIMULINK model as shown in Fig. 4.

The Longitudinal Wheel block implements the longitudinal behavior of an ideal wheel. You can specify the longitudinal force and rolling resistance calculation method, and brake type. Use the block in driveline and longitudinal vehicle simulations where low frequency tire-road and braking forces are required to determine vehicle acceleration, braking, and wheel-rolling resistance. For example, you can use the block to determine the torque and power requirements for a specified drive cycle or braking event. The block is not suitable for applications that require combined lateral slip. The block calculates the inertial response of the wheel subject to: Axle losses, Brake and drive torque, Tire rolling resistance and ground contact through the tire-road interface. The input torque is the summation of the applied axle torque, braking torque, and moment arising from the combined tire torque.

$$\mathrm{Ti} = \mathrm{Ta} - \mathrm{Tb} + \mathrm{Td} \tag{10}$$

For the moment arising from the combined tire torque, the block implements tractive wheel forces and rolling resistance with first order dynamics. The rolling resistance has a time constant parameterized in terms of a relaxation length.

$$\mathrm{Td} = \omega \mathrm{ReLe} + \omega \mathrm{Re}(\mathrm{FxRe} + \mathrm{My}) \tag{11}$$

To calculate the rolling resistance torque, we the method in Stepwise Coast down Methodology for Measuring Tire Rolling Resistance. The rolling resistance is a

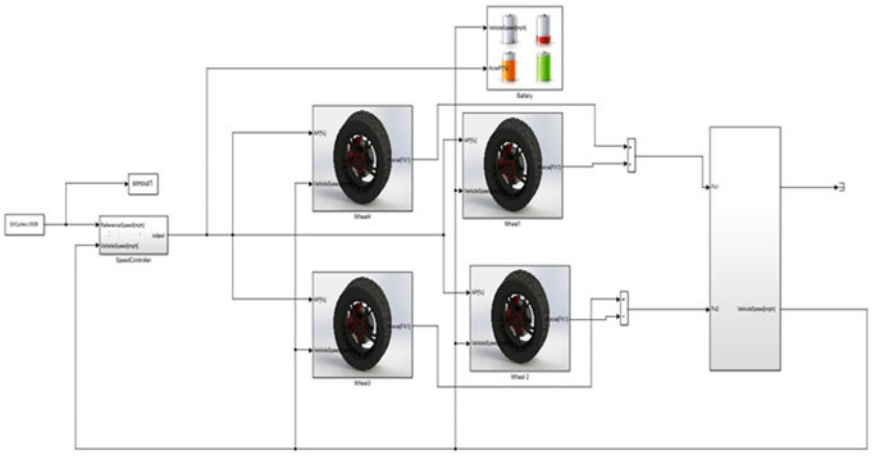

Fig. 4 Simulink block diagram of robot control

Table 1 Simulation parameters 1

If	Lock-up condition	Friction model
$\omega \neq 0$ or TS $<$ |Ti + Tf − ωb|	Unlocked	Tf = Tk Where $Tk = F_C R_{eff} u_k \tanh[4(-w_d)]$ $Ts = F_C R_{eff} u_s$ $R_{eff} = \frac{2(R_0^3 - R_i^3)}{3(R_0^2 - R_i^2)}$
$\omega = 0$ and TS $\geq$ |Ti + Tf − ωb|	Locked	Tf = Ts

Table 2 Simulation parameters 2

If	Lock-up condition	Dynamic model
$\omega \neq 0 or TS < \|Ti + Tf - \omega b\|$	Unlocked	$\omega_j = -\omega_b + Ti + To$
$\omega = 0 \; and \; TS \geq \|Ti + Tf - \omega b\|$	Locked	$\omega = 0$

function of tire pressure, normal force, and velocity. Specifically:

$$M_y = R_e\left\{a + b|V_x| + cV_x^2\right\}\left\{F_Z^B p_i^a\right\}\tanh(4V_x) \tag{12}$$

If the brakes are enabled, the block determines the braking locked or unlocked condition based on an idealized dry clutch friction model. Based on the lock-up condition, the block implements these friction and dynamic models (Tables 1 and 2).

The equations use these variables (Table 3).

The robot RAMBLER uses the Brake Type Disc, the block implements a disc brake. A disc brake converts brake cylinder pressure from the brake cylinder into force. The disc brake applies the force at the brake pad mean radius. The block uses these equations to calculate brake torque for the disc brake.

$$T = \begin{cases} \frac{\mu p \pi B_a^2 R_m N_{pads}}{2} & \text{when } N \neq 0 \\ \frac{\mu_{static} p \pi B_a^2 R_m N_{pads}}{4} & \text{when } N = 0 \end{cases} \tag{13}$$

$$R_m = \frac{(R_0 + R_i)}{2} \tag{14}$$

The equations use these variables (Table 4).

5 Simulation

The simulation of the controller is done by an implementation on model of robot of the type with the aid of Toolbox of the Simulink, we tested the robot capability of the reference speed tracking. We have made three simulations with different parameters shows as follows (Table 5).

Table 3 Description of parameters

Variables	Description
ω	Wheel angular velocity
a	Velocity independent force component
b	Linear velocity force component
c	Quadratic velocity force component
Le; My	Tire relaxation length; Rolling resistance torque
Ta; Tb	Applied axle torque; Braking torque
Td	Combined tire torque
Tf; Ti	Frictional torque; Net input torque
Tk	Kinetic frictional torque
μk	Coefficient of kinetic friction
To; Ts	Net output torque; Static frictional torque
Fc; Fx	Applied clutch force; Longitudinal force
Reff	Effective clutch radius
Ro; Ri	Annular disk (outer radius; inner radius)
Re	Effective tire radius
Vx; Fz	Vehicle normal force; Longitudinal axle velocity
α; β	Tire pressure and Normal force exponent
pi; μs	Tire pressure; Coefficient of static friction

Table 4 Variables of equations

Variables	Description
T	Brake torque
P	Applied brake pressure
N	Wheel speed
Npads	Number of brake pads in disc brake assembly
μstatic	Effective clutch radius
μ	Disc pad-rotor coefficient of kinetic friction
Ba	Brake actuator bore diameter
Rm	Mean radius of brake pad force application on brake rotor
R0	Outer radius of brake pad
Ri	Inner radius of brake pad

Table 5 Variables of equations

Simulation	Vehicle mass KG	Absolute pressure, Pabs [Pa]:	Kinetic friction coefficient
Simulation 1	1000	1325	0.8
Simulation 2	1500	2000	2
Simulation 3	3000	5000	5

The figures below show the speed of the robot and the evolution of the control variables according to time.

The figures Figs. 5, 6 and 7 obtained with simulation 1. The figures Figs. 8, 9, 10 and 11 obtained with simulation 2. The figures Figs. 12, 13, 14 and 15 obtained with simulation 3. With the obtained results we can noted, that our control design is robust and system is stable. the error is small and vehicle tacking trajectory in real time. But with high perturbation (variation of parameters) like in simulation 3, we need amore robust controller like Fractional order PID controller.

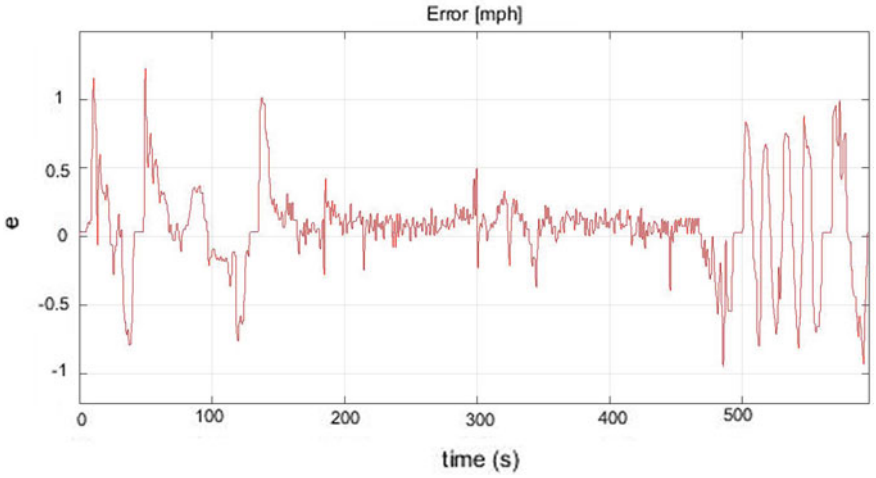

Fig. 5 Curve of error (Simulation 1)

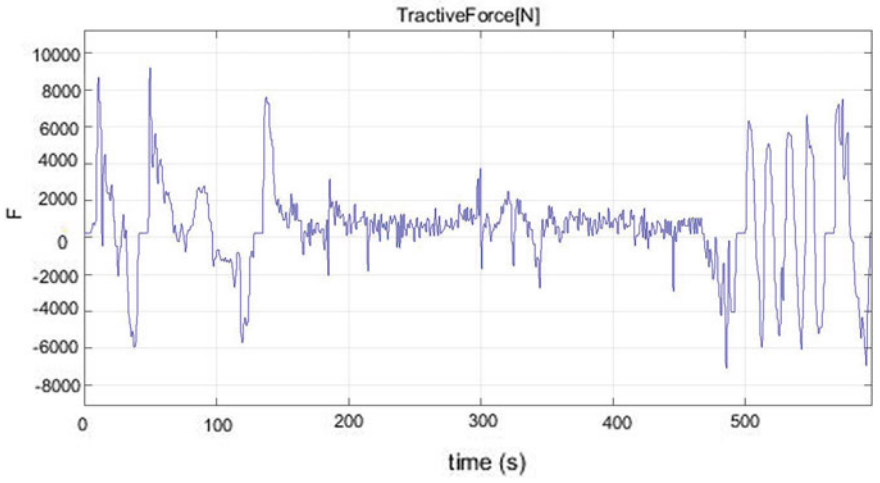

Fig. 6 Curve of force (Simulation 1)

Fig. 7 Curve of speed vehicles (Simulation 1)

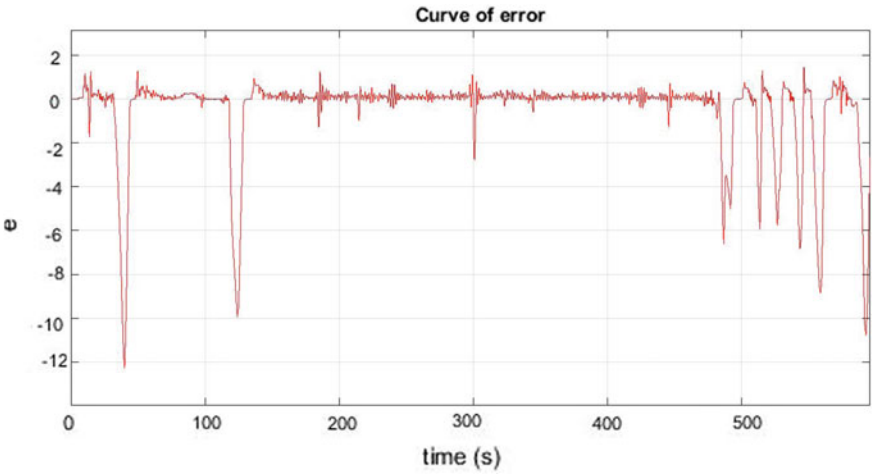

Fig. 8 Curve of error (Simulation 2)

6 Conclusion

In this paper we proposed path tracking controller for an autonomous vehicle with four wheels, the controller is based PID, is able to offer more tracking flexibility. After several testes that we did we noticed that the starting point and the initial orientation influenced on the trajectory tracking, for this reason we have to choose the initial condition to decrease the value of the error, the proposed model can be also used in the platooning projects (train of vehicles leader-follower), with different design of control based in multi-architecture controller with different type of controller more

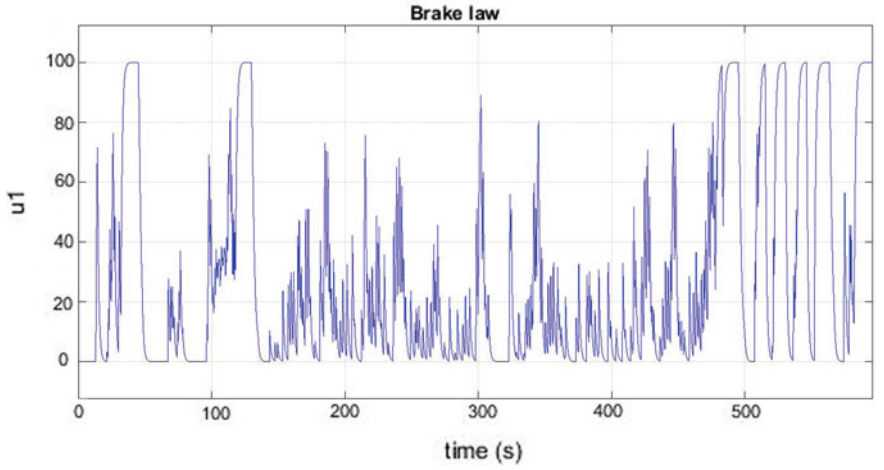

Fig. 9 Curve of brake (Simulation 2)

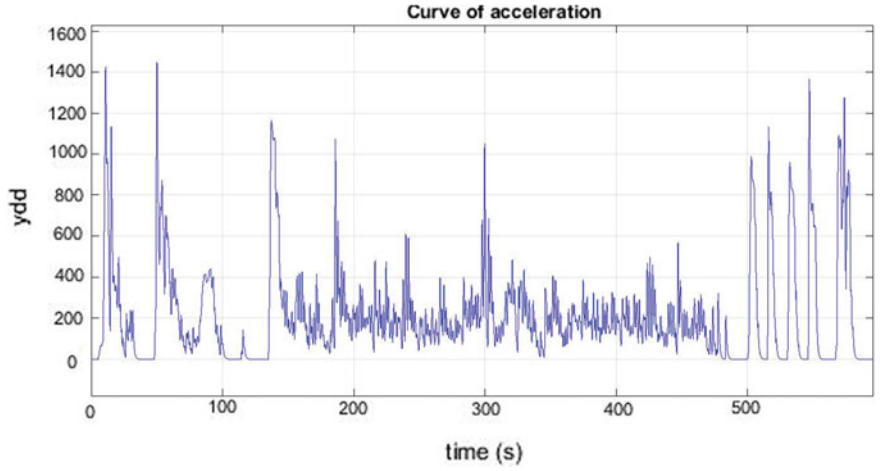

Fig. 10 Curve of acceleration (Simulation 2)

robust and optimizing with PSO, Genetic Algorithm, Wolf algorithm… In the future works we plan, to integrate the proposed method to achieve a train of vehicles.

General characteristics of vehicles:

- Dimensions: 1.6 m length, 1.2 m width, 0.66 m height.
- Vehicle weight: 370 kg.

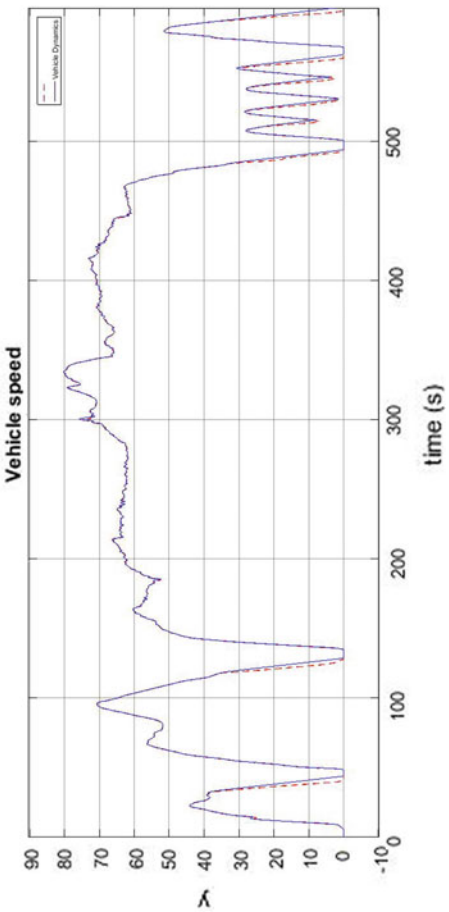

Fig. 11 Curve of speed vehicles (Simulation 2)

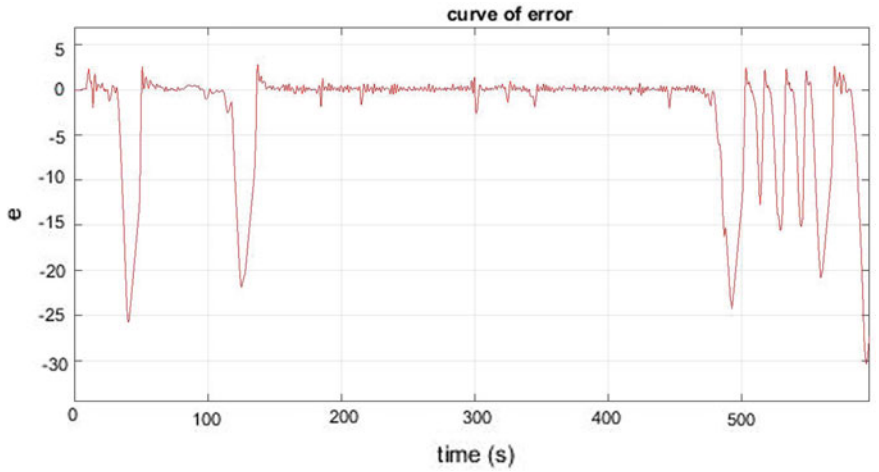

Fig. 12 Curve of error (Simulation 3)

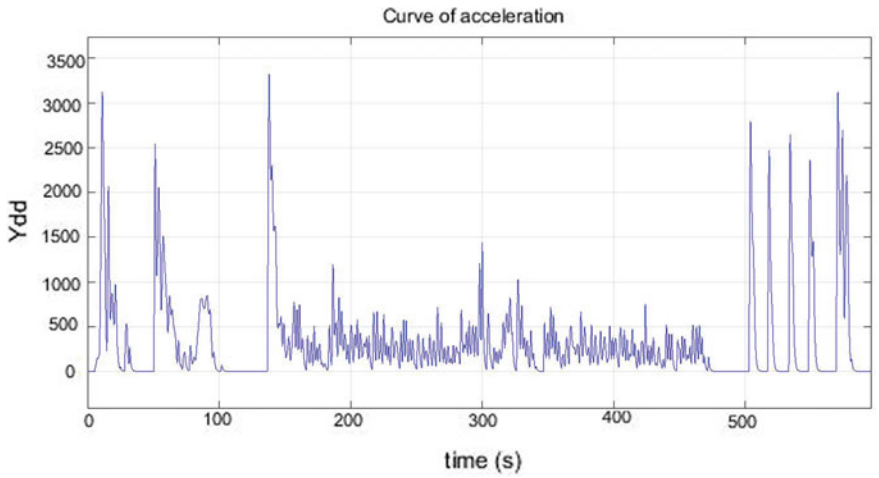

Fig. 13 Curve of acceleration (Simulation 3)

- Payload: >320 kg.
- Distance between the front and rear wheel contact points: From 0.95 to 1 m.
- Wheels: pneumatic tires of 50 cm diameter.
- Suspension: Active/Semi active suspension system. Pneumatic.
- Distance between left and right wheel contact points is L = 1.05 m.
- Maximum linear speed: 80 km/h, 22.2 m/s.
- Battery: (LiFePO4); Range 44,8 < V < 59,2; 160 Ah (4 cells × 40 Ah); Configuration:16S4P. Temperature: 0 °C < t < 70 °C. Operativo Control: BMS.

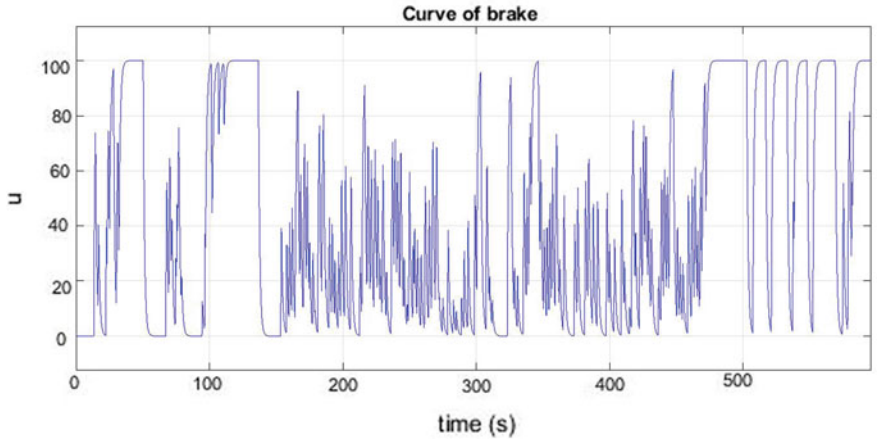

Fig. 14 Curve of brake (Simulation 3)

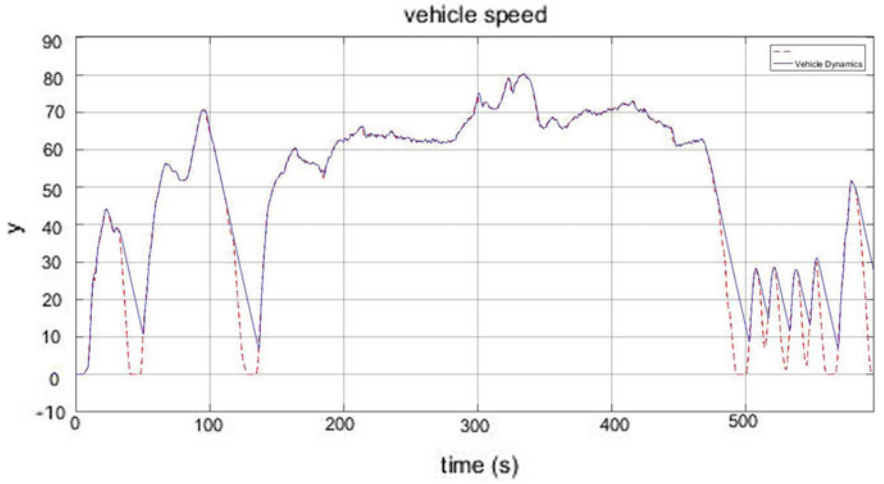

Fig. 15 Curve of speed vehicles (Simulation 3)

contactor 600A/80eVdc SPST-NO (Normally Open). Charge Control: External, 59,2 V/80 A, 4,7 kW.

- Motors: Brushless DC Electric Motor with Outrunner Configuration.
- Range: 36–72 Vdc, 500–3000 W. Nominal speed: 300–1000 rpm.

Acknowledgments The authors wish to thank the project DPI2015-65186-R, funded by the Spanish Government, for the availability of the robot RAMBLER for this work.

References

1. https://www.uma.es/robotics-andechatronics/info/107721/FIRST-ROB/, (consulted 20/10/2018)
2. Baturone I, Sánches-Solano FJS, Ollero A (2004) Automatic design of fuzzy controllers for car-like autonomous robots. IEEE Trans Fuzzy Syst 12(4):447–465
3. García C, Strang T, Lehner A (2008) A broadcast vehicle to vehicle communication system in railway environments. ISVCS 2008, Dublin, Ireland, p 6
4. Bingyi L, Kejie J, Dong LN, Jianping W, Libing W (2017) A joint control-communication design for reliable vehicle platooning in hybrid traffic. IEEE Trans Veh Technol 66(10):9394–9409
5. Fernandes P (2010) Platooning of autonomous vehicles with intervehicle communications in SUMO traffic simulator. In: 13th IEEE international conference on intelligent transportation systems, Portugal, pp 1313–1318
6. Cao Y, Liu S, Visual Servo Control for wheeled robot platooning based on homography. In: 6th data driven control and learning system, pp 628–632
7. Messaoudène K, Azouaoui O (2015) Personalized dynamic model for a car-like vehicle "Robu-car" used in localization. In: IEEE international conference on systems, man, and cybernetic, pp 2533–2538
8. Campolo C, Mlinaro A, Araniti G, Berthet AO (2017) Better platooning control toward autonomous driving: an LTE device to-device communication that meets ultralow latency requirements. IEEE Veh Technol Mag 12(1):30–38
9. Ploeg J, Vande WOuw N, Nijmeijer H (2014) Lp string stability of cascaded systems/application to vehicle platooning. IEEE Trans Control Syst Technol 22(2):786–793
10. Dumont P-E (2006) Tolérance active aux fautes des systèmes d'instrumentation, vol 1. Thèse doctorat, université Lille, p 163
11. Bouibed K (2010) Contribution à la gestion de défaillances d'un train de véhicules électriques légers autonomes, vol 1. Thèse doctorat, université Lille, p 181
12. Al-Mayyahi A (2015) Path tracking of autonomous ground vehicle based on fractional order PID controller optimized by PSO. In: IEEE 13th international symposium on applied machine intelligence and informatics, Slovakia, pp 109–114
13. Turki YA, Abdulkareem AA (2012) PSO-based optimum design of PID controller for mobile robot trajectory tracking. Int J Comput Appl 47(23):30–35
14. Al-Mayyahi A, Wang W, Birch P (2015) Design of fractional-order controller for trajectory tracking control of a non-holonomic autonomous ground vehicle. Int J Control Autom Electr Syst 14
15. Al-Mayyahi A, Wang W, Birch P (2014) Adaptive neuro-fuzzy technique for autonomous ground vehicle navigation. Robotics, pp 349–370
16. Zoleikha AB, Satadru D, Pisu P (2017) Real-time detection and estimation of denial of service attack in connected vehicle systems. Ieee Trans Intell Transp Syst Xx(X):11
17. Allou S, Zennir Y, Belmeguenai A (2017) Fuzzy logic controller for autonomous vehicle path tracking. In: 18th international conference on sciences and techniques of automatic control & computer engineering—STA'2017, Monastir, Tunisia, pp 328–333
18. Zennir Y, Mechhoud E, Seboui A, Bendib R (2017) Multi-controller approach with PSO-PIλDμ controllers for a Robotic Wrist. In: The 5th international conference on electrical engineering—boumerdes (ICEE-B), Boumerdes, Algeria, p 7